REVISION 1

Towards the wider application of ^{29}Si NMR spectroscopy to paramagnetic transition metal silicate minerals: copper(II) silicates

Jonathan F. Stebbins

Department of Geological Sciences, Stanford University, Stanford CA 94305

stebbins@stanford.edu

Running title:

"NMR of paramagnetic copper silicates"

ABSTRACT

^{29}Si NMR has only rarely been applied to silicate minerals in which the predominant cations have unpaired electron spins (e.g. most transition metals and REE), because of the potential for serious line broadening and signal loss. However, as shown here, spectra for a series of natural and synthetic copper(II) silicate minerals can be readily obtained, have paramagnetic shifts far outside known chemical shift ranges, and potentially are very sensitive to structural details involving interactions of paramagnetic cations and Si sites. Signals from different silicon sites in the structures can be distinguished and quantified. Peak broadening due to magnetic couplings and to disorder can be large, but not to the point of 'non-observability'. NMR signal loss can be related to specific, and in some cases improvable, technical issues such as excitation bandwidth, sample spinning speed, and rapid nuclear spin relaxation. Two samples of the 'mineraloid' chrysocolla from different copper ore deposits have very similar spectra with significant paramagnetic shifts, suggesting strong Si-Cu interactions and a common stoichiometry and short-range structure.

Keywords:

nuclear magnetic resonance, unpaired electron spins, dioptase, shattuckite, cuprorivaite, planchéite, chrysocolla

INTRODUCTION

Since the earliest applications of high resolution, magic-angle spinning (MAS) ^{29}Si NMR to minerals in the late 1970's and early 1980's, nearly all studies have been on materials with low (< a few %) contents of paramagnetic cations, whose unpaired electron spins can interact strongly with nuclear spins and can cause severe NMR line broadening, sometimes to the point

of making signal difficult or even impossible to observe with conventional methods (Engelhardt and Michel 1987; Grimmer et al. 1983; MacKenzie and Smith 2002). This problem (actual or expected) has generally limited application of this powerful experimental technique to groups of minerals with low natural contents of transition metal and rare earth cations (e.g. feldspars, feldspathoids, zeolites, silica polymorphs, clays, white micas, etc.) or to end members of ferromagnesian solid solutions, often synthetic, with low or no Fe^{2+} or other transition metal cations (e.g. olivines, pyroxenes, amphiboles, high pressure mantle phases, etc.).

However, paramagnetic interactions can also cause large, but observable, changes in NMR peak positions far outside the ranges for diamagnetic materials, as has been particularly well-studied for ^{6,7}Li and ^{31}P NMR in Li-rich transition metal oxides and phosphates of major interest in advanced battery materials (Carlier et al. 2003; Grey and Dupré 2004; Tucker et al. 2002). In such materials, despite paramagnetic shifts of thousands of ppm and sometimes severe line broadening, both simple MAS NMR and more advanced methods have revealed important new details about ordering of cations, bonding, site symmetries, and other details of short range structure (Strobridge et al. 2014; Yoon et al. 2004; Zeng et al. 2007). This extended work has led to considerable advances in the theoretical understanding of the complex physics behind such interactions, as well as a rapidly developing ability to calculate paramagnetic shifts from first principles (Clément et al. 2012; Middlemiss et al. 2013). ^{31}P MAS NMR for many pure-phase rare earth monazite-type or zircon-type phosphates are also readily observable, again with paramagnetic shifts of up to 100's of ppm depending on the number of unpaired spins and details of the electronic structure (Bose et al. 1979; Bregiroux et al. 2007). Pioneering studies of ^{119}Sn and ^{89}Y MAS NMR in rare earth stannate pyrochlores introduced this approach to mineralogically interesting oxides (Grey et al. 1989; Grey et al. 1990); very recent studies have

reported highly shifted ^{25}Mg (Lee et al. 2017) and ^{27}Al (Dogan et al. 2016) resonances in spectra in doped transition metal oxide battery materials and in ^{89}Y and ^{137}Ba NMR data for transition metal perovskite phases (Michaelis et al. 2012). Of particular interest in geochemistry are studies of sorbed lithium and phosphate on iron oxyhydroxides, where ^{7}Li and ^{31}P NMR spectra are strongly affected by the host Fe^{3+} cations (Kim et al. 2011; Kim et al. 2008).

In contrast, very few NMR studies of pure-phase paramagnetic transition metal silicates have been reported with a rare exception of early work on Co_2SiO_4 (Saji et al. 1973). However, recent reports on synthetic olivine and natural garnet solid solutions containing 0.1 to 20% FeO, NiO, or CoO have shown that, at least in such fairly dilute systems, useful resolution can be observed for Si sites with one or two paramagnetic first-neighbor cations, with shifts up to about 400 ppm above the known chemical shift range of –60 to –120 ppm (Begaudeau et al. 2012; McCarty et al. 2015; Palke and Stebbins 2011a; Palke et al. 2015; Stebbins and Kelsey 2009; Stebbins et al. 2017).

Such paramagnetic shifts in NMR peaks can be either positive or negative, and are caused by a through-bond transfer of unpaired electron spin density ("Fermi contact shift") and/or a through-space dipolar coupling from a magnetic cation in an asymmetrical site ("pseudocontact shift") (Grey et al. 1989; Grey et al. 1990; Bertini et al. 2002; MacKenzie and Smith 2002). These two mechanisms have been recently discussed in the mineralogical context of rare-earth containing phosphate minerals and garnets (Palke and Stebbins 2011a,b; George et al. 2013; McCarty and Stebbins 2016). The Fermi contact shift (also known as the "transferred hyperfine coupling" when the unpaired electron spin is associated with an ion different from that under observation by NMR) involves perturbation of the electron spin density by transfer through one or more chemical bonds, and hence depends strongly on the degree of covalency in

the bonds (hence, their length) between the paramagnetic ion and the observed NMR nuclide. This interaction can sometimes be detected several bonds away, but falls off rapidly with the number of intervening bonds. It depends strongly as well on the nature and extent of orbital overlap, which in turn are affected by the intervening bond angles and coordination environments for both the paramagnetic center and the observed nuclide, and on the gyromagnetic ratio γ of the NMR nuclide. In contrast, the pseudocontact shift mechanism involves the direct, through-space magnetic dipolar coupling between the unpaired electron spin and the nuclear spin, and hence falls off as the inverse cube of their separation. This effect on the NMR resonance frequency is controlled by the anisotropy of the magnetic susceptibility tensor for the paramagnetic center, which can vary widely in magnitude and symmetry depending on the local structure, and is not averaged away by magic angle spinning. This tensor can sometimes be measured by EPR spectroscopy; it may also be closely related to crystal field effects in optical spectroscopy (e.g. George et al. 2013).

In some cases, the predominant shift mechanism can be deduced from geometric considerations, areas and numbers of shifted peaks and approximate estimations (Grey et al. 1989; Grey et al. 1990; Palke and Stebbins 2011a,b); as noted above there has been considerable recent progress towards more quantitative calculation for transition metal phosphates and oxides. For a given site in a mineral, both may be important. However, in spite of such theoretical advances, prediction of such shifts remains challenging, and little is known about what to expect in silicates where paramagnetic components are predominant instead of dilute, beyond the obvious guesses that shifts will be large and peak broadening may be severe. The much lower resonant frequency (due to the lower gyromagnetic ratio γ) of ^{29}Si relative to better-studied ^{7}Li and ^{31}P (Stebbins and Xue 2014), and even more importantly its much lower natural isotopic

abundance (4.7% vs. 93% and 100% respectively) will both lower sensitivity (i.e. obtainable signal to noise ratio) significantly; however the lower γ of ^{29}Si will also reduce the strength of electronic-nuclear dipolar couplings, which can be a major contributor to line broadening in paramagnetic materials.

An obvious and important first step in the better understanding of the effects of paramagnetic cations in ^{29}Si NMR spectra of transition-metal rich silicate minerals, and hence potentially a more wide applicability of this method to large groups of natural minerals and technological materials, will be to determine whether such spectra for pure-phase end member compositions are in fact observable and whether they suggest that useful structural information can be obtained. Cu^{2+} offers an intriguing, and as-yet unexplored, entry point, as the single unpaired electron in this cation may reduce the interaction and line broadening relative to the effects of other divalent transition metals, e.g. the four unpaired spins for high-spin Fe^{2+}. At the same time, the coordination environment of Cu^{2+} in most silicates (square planar or square planar with two more distant neighbors such as H_2O) is distinct from more common octahedral environments more commonly found for Fe^{2+}, etc. Here it is demonstrated for the first time that useful ^{29}Si NMR spectra can indeed be observed for a series of natural and synthetic Cu^{2+} silicates, and that these are sensitive to local structure and composition, although all of the data cannot yet be interpreted in detail. ^{29}Si NMR can also provide new insights into the structure of the common, but problematical Cu^{2+} silicate chrysocolla, which is often X-ray "amorphous," but is considered by some researchers to be a "mineraloid" with considerable short-range order and consistent stoichiometry (Farges et al. 2007; Frost et al. 2012).

SAMPLES AND EXPERIMENTAL METHODS

Natural mineral samples were from the Stanford University Research Mineral Collection, (Tab. 1), with identities confirmed by powder XRD. Electron microprobe analyses showed that both dioptase samples had nearly ideal composition, although a minor calcite impurity was detected in some fragments of the Altyn Tyube sample. The shattuckite samples were also of near-ideal composition, with only minor quartz impurities. The soft, fibrous nature of the planchéite resulted in a relatively poor polish, but EPMA data gave a systematically low atomic Cu/Si ratio of about 0.85 (vs. 1.0 ideal), probably because of the presence of about 1.5 wt% K_2O, 0.5% Na_2O and 3% MgO, suggesting possible K^+, $Na^+$and Mg^{2+} substitution on the M sites of this amphibole-like structure (Evans and Mrose 1977). EPMA and optical microscopy also revealed that some fragments of this material had minor amounts of coarse particles of an iron oxide phase, probably hematite. Most of this contaminant was removed from the NMR sample by hand picking. Both chrysocolla samples were massive and uniformly blue-green in color, with earthy lusters and without obvious color banding or other heterogeneities.

Some of the dioptase was dehydrated by heating a powder at 600 ˚C for 1 h, which gave the expected weight loss and yielded a black material as previously reported (Law et al. 2010) with an XRD pattern as in previous studies (Breuer and Eysel 1989). Synthetic cuprorivaite ("Egyptian blue" pigment) was synthesized in air from a stoichiometric mixture of CuO, $CaCO_3$, and amorphous SiO_2 with 1 wt% Na_2CO_3 as a flux, heated for 23 h at 1000 ˚C (Bloise et al. 2016; Chakoumakos et al. 1993; Pradell et al. 2006). (The flux is helpful in allowing more complete reaction at the relatively low synthesis temperatures needed to maintain Cu in the divalent state.) The product was the expected deep blue color. EPMA indicated that about 95% of the material formed coarse grains that had the correct stoichiometry, with the remainder of the

sample present as unreacted silica, Ca-rich silicates or Na-rich material remaining from the Na fluxing process. Powder XRD on this material detected only cuprorivaite (Chakoumakos et al. 1993) and traces of cristobalite; optical microscopy indicated that much of the non-cuprorivaite material was amorphous, presumably residual glass.

NMR spectra were collected with a Varian 400 MHz spectrometer, at 79.5 MHz for ^{29}Si, with 3.2 mm MAS rotors, spinning at 10 to 20 kHz or non-spinning ('static'). Frequencies are referenced to TMS at 0 ppm. To observe broad peaks a spin-echo pulse sequence (90˚- τ - 180˚) was used with the delay time τ of 50 to 100 μs to match an integral number of rotor periods and to shift most of the NMR signal away from residual probe "ringing", an instrumental artifact that is a source of what is essentially additional noise immediately after the last transmitted observe pulse, in this system lasting a few 10's of μs. A 90˚ pulse length of 3 μs led to a relatively small excitation bandwidth (ca. 150 kHz), and required moving the transmitter frequency by up to several 1000's of ppm to initially locate the resonances and then to accurately observe spectra. For the main NMR peaks of the Cu-silicates, relaxation was very rapid and allowed quantitative spectra to be obtained with pulse delays of 0.1 s and total acquisition times of 3 to 20 h. Signals for minor diamagnetic impurities relaxed more slowly and were observed with longer pulse delays; their spectral components may be under-represented when not fully relaxed. Peak areas, normalized to the nominal amount of SiO_2 in each sample, were ratioed to that of a pure natural diopside (Wakefield, Quebec), the latter observed with a pulse delay of 1 h to ensure full relaxation. Temperatures due to air frictional heating were measured from the ^{207}Pb NMR peak shift in $Pb(NO_3)_2$ (Takahashi et al. 1999) as 31±2 ˚C at 10 kHz and 57±2 ˚C at 20 kHz. Even this small difference produced large changes in positions of peaks with high paramagnetic shifts; thermal gradients in rotors probably also increased the widths of the narrower peaks.

RESULTS AND DISCUSSION

Dioptase

Table 1 gives NMR peak maxima, widths (full width at half maximum, FWHM), and normalized peak areas. Dioptase ($Cu_6Si_6O_{18} \cdot 6H_2O$) has a simple, well-known structure with rings of six SiO_4 tetrahedra and a single Si site (with two bridging and two non-bridging oxygens, or "Q^2"), each with four closest Cu^{2+} neighbors in square planar coordination with two more distant H_2O molecules (Ribbe et al. 1977). As in shattuckite and planchéite (below), each Cu^{2+} shares at least one oxygen with another Cu^{2+} cation, forming continuous copper oxide chains. The single ^{29}Si NMR peak of dioptase (+980 ppm at 20 kHz spinning rate, ca. 57 ˚C) is shifted far outside of the known range for diamagnetic silicates, i.e. –60 to –120 ppm (Fig. 1). Effects of spinning rate on sample temperature, and hence on peak position, are well illustrated by this mineral (Fig. 2) and are as expected for a large paramagnetic shift (Palke and Stebbins 2011). For these and other samples, the effects of temperature (T) on the shift scale with the magnitude and sign of the shift as expected, and extrapolate roughly to the normal diamagnetic chemical shift range when extrapolated to 1/T = 0. Dioptase samples from two different localities had nearly identical spectra. Peak widths are among the narrowest observed for these copper silicates (2 to 4 kHz or 25 to 40 ppm, in contrast to <1 ppm for ordered, diamagnetic silicates), but are clearly affected by thermal gradients in the rotors, especially at the faster spinning speeds. When data are collected with the spectrometer frequency centered on the resonance, integrated peak areas (including spinning sidebands) are within 95% of values expected by intensity calibration with the diopside standard, showing minimal loss of signal during the 50 to 100 μs echo delay. This in turn indicates that the spin-spin relaxation time T_2 is much larger than the echo delay. The sidebands, especially when made more prominent by slower spinning (Fig.

2), map out the pattern observed without spinning, with an additional shift with temperature decrease from about 31 ˚C at 10 kHz to about 24 ˚C without spinning. The static (non-spinning) line shape resembles that produced by chemical shift anisotropy in a diamagnetic silicate, indicating an orientation dependence to at least one part of the paramagnetic coupling (probably the through-space dipolar interaction) between the unpaired electrons of Cu^{2+} and the ^{29}Si nuclear spins.

The spectrum for dehydrated dioptase ($Cu_6Si_6O_{18}$, not the metastable $CuSiO_3$ chain silicate that can be produced at higher temperatures) is slightly broader with a paramagnetic shift about 85 ppm lower, but both MAS and static spectra are overall quite similar to those of the original, hydrated material: this change in position is relatively small given the >1600 ppm total shift range observed for copper silicates (Fig. 2). Dehydrated dioptase has been extensively studied because of its unusual low temperature magnetic properties (Law et al. 2010) and, apart from the loss of the H_2O molecules, has a crystal structure nearly identical to that of the hydrous phase, with slightly shorter Cu-O and slightly longer Si-non-bridging oxygen bonds. Although the color change from brilliant green to black on dehydration does suggest an important change in the electronic structure around the Cu^{2+} ion, this change apparently does not strongly affect either the crystal structure or the paramagnetic shift in the ^{29}Si NMR spectrum, probably because in the hydrated material the H_2O molecules interact only weakly with the SiO_4 groups, but do add two distant oxygens to the CuO_4 groups to form stretched "4+2" octahedra.

Detailed studies of Li-rich transition metal phosphates (e.g. $LiMPO_4$, with M=Fe^{2+}, Ni^{2+}, Co^{2+}, most commonly with the olivine structure) have shown that paramagnetic shifts for their ^{31}P spectra are dominated by through-bond Fermi contact shifts (Middlemiss et al. 2013; Strobridge et al. 2014), primarily (but not exclusively) from the first neighbor cations, and that

the observed total shift can be well approximated by the sum of observed and/or calculated shifts for each individual M-O-P bond pathway. The electronic structure of the paramagnetic cation in its site (or sites) in the structure is critical; the number of unpaired electron spins is important but, surprisingly, not always predominant in the magnitude of the shift. The magnitude and even the sign of the Fermi contact shift for a given bond pathway depend sensitively on the degree of covalency and orbital overlap, which can be reflected in the bond distances and especially in the M-O-P bond angles, in turn affected by cation coordination number and geometry. This complex picture is likely to apply to transition metal-rich silicates as well, as the non-bridging oxygens on the SiO_4 groups, each coordinated by one or more paramagnetic transition metal cations, are at least roughly analogous to those in the PO_4 groups of the phosphates.

The observed paramagnetic shift for dioptase (about +980 ppm at ca. 57 ˚C) might thus be approximated as resulting predominantly from the sum of through-bond electron spin transfer along four distinct bond pathways to the four first neighbor Cu^{2+} cations, each having one unpaired electron spin. Two such pathways go through each of the two non-bridging oxygens in the structure (O2 and O3). Cu-O and Si-O distances along each fall within a small range, as do the four Cu-O angles, which vary from 119 to 132˚ (Ribbe et al. 1977). It is also important to note that in contrast to the more regular octahedral coordination of other transition metal cations in well-studied Fe-, Mn-, Co-containing battery materials (Li-rich oxides and phosphates), the large geometric anisotropy of the CuO_4 groups (which may also have two additional distant apical oxygens in some Cu silicates) is likely to generate a large magnetic anisotropy as well. This could contribute to significant through-space pseudo-contact shifts in addition to the surmised large, through-bond Fermi contact shift. At this time, however, it is not possible to interpret these new results on copper silicates in more detail.

Shattuckite

Shattuckite ($Cu_5(SiO_3)_4(OH)_2$), can, like dioptase, be obtained in coarse, monomineralic form and has a well-determined structure (Evans and Mrose 1977). Its single-chain structure has two distinct Q^2 Si sites in equal populations (Fig. 3). Si1, which resembles the Si site in dioptase, has four CuO_4 closest neighbors, two for each non-bridging oxygen with Cu-O-Si angles of 109 to 121˚. Si2, in contrast, has three close (Cu-O-Si of 126 to 128 ˚) and two distant CuO_4 neighbors (Cu-O-Si of 110 and 132˚). Two relatively narrow NMR peaks are observed (Fig. 1), with equal areas each comprising nearly 50% of that expected from the diopside standard. Again, both shifts for this phase are far outside of the known range for chemical shifts, one above, one below. The spectrum shown in Fig. 1 was collected with the transmitter frequency halfway between the two resonances, which substantially reduced the intensities of both because of limited excitation bandwidth. Data for area quantification were collected with the frequency centered on each peak separately; the latter spectra also showed more symmetric spinning sideband patterns, resembling those observed for dioptase. The apparently asymmetric sideband patterns for both peaks in the shattuckite data in Fig. 1 are not the consequence of an especially anisotropic shift interaction, but instead illustrate the drop-off in intensity away from the center of the spectrum, caused by the limited excitation bandwidth of the echo pulse sequence used. The higher frequency peak in shattuckite is significantly broader than the low frequency peak, and than the peak in dioptase. Whether this is a consequence of disorder (e.g. in H positions) or an effect of differential relaxation is not yet known.

The observed shift at +1580 ppm (peak A) can be tentatively assigned to Si1, whose large positive shift is somewhat comparable to that in dioptase, and that at –250 ppm (peak B) to Si2

because of the smaller number of short Cu-O-Si bond pathways in the latter, but further study will be needed to confirm this hypothesis. Note that both positive and negative paramagnetic shifts can be induced by a given paramagnetic cation, depending on the details of orbital geometry, electron distributions in bonds (Middlemiss et al. 2013), and the relative roles of Fermi contact shifts and, potentially, of pseudocontact interactions. OH^- groups in this phase (and planchéite, below) may also significantly alter electronic distributions, if they change the covalency of other Cu-O bonds linked to Si and thus extent of the electronic spin transfer.

Planchéite

The structure of planchéite ($Cu_8(Si_4O_{11})_2(OH)_4 \cdot xH_2O$, $x \approx 0.43$) is considered to be less precisely known than, but related to, that of shattuckite, with some difficulty in the structure determination due to the fine grained, fibrous nature of the mineral (Evans and Mrose 1977). The material studied here, a massive, uniformly colored greenish blue material from the copper mining district in Guchab, Namibia, was comprised of a dense aggregate of fibrous material and had a powder XRD pattern that matched that in the JCPDS data base, from data in Evans and Mrose (1977). EPMA data indicated, however, that up to about 10% of the Cu^{2+} was replaced by Mg^{2+}, K^+ and Na^+, potentially increasing the disorder in the structure. The published structure has a double silicate chain, and 4 inequivalent Si sites, with equal proportions of Q^2 (Si1, Si4) and Q^3 (Si2, Si3) tetrahedra. The former appear to each have four CuO_4 neighbors as in dioptase, the latter probably with two Cu neighbors each. Initially only the NMR peak labeled "B" was observed (Fig. 1), paramagnetically shifted to +130 ppm but with a much broader line (19 kHz) than that for dioptase or shattuckite. Sample spinning rate was insufficient to narrow this completely. After testing a range of transmitter frequencies, a second, even broader (≈70 kHz)

peak "A" was detected centered at about 1200 to 1400 ppm. It is likely that some type of disorder or poor crystallinity in this fibrous, fine-grained mineral contributes to broadening of both peaks. The spectrum shown in Figure 1 was collected with the transmitter frequency midway between the two peak maxima. By analogy to the spectra for shattuckite, peak A can be tentatively assigned to the Q^2 sites (more Cu neighbors, strongly total magnetic interaction) and peak B to the Q^3 sites, but again further study will be required to confirm this.

With the standard echo delay of 100 μs, the overall integrated area (both peaks) is about 74% of that expected from the diopside standard. This value was only slightly higher (76%) at the minimum practical echo delay of 50 μs (Fig. 4), indicating that the "missing" observed intensity is not solely the result of signal decay (spin-spin relaxation) during the pulse sequence, but is more likely dominated by insufficient excitation bandwidth. Given peak overlap and unconstrained peak shapes, fitting of the spectra to obtain relative areas has low accuracy, but the broader "A" peak could plausibly account for half of the total as expected from our tentative assignment to the Q^2 sites in this structure.

In the planchéite spectra, a small, much narrower third peak ("D") was also detected, whose position may be consistent with a small or negligible paramagnetic shift, suggesting the presence of a minor unknown impurity phase undetected by XRD or EPMA.

Cuprorivaite ("Egyptian blue")

Among the known anhydrous copper silicates, cuprorivaite ($CaCuSi_4O_{10}$) appears to be relatively straightforward to synthesize. It is the main constituent of the "Egyptian blue" pigment invented millennia ago, apparently as a simulant for the prized lapis lazuli gemstone (Pabst, 1959), and also occurs rarely in nature.

The structure of cuprorivaite has corrugated silicate sheets with a single Q^3 Si site (Chakoumakos et al. 1993), CuO_4 square planar coordination and only a single Cu^{2+} first neighbor to each Si (Fig. 3). The relatively large paramagnetic shift of +720 ppm (Fig. 1) is thus somewhat surprising, but this phase does have underbonded non-bridging oxygens and a resulting unusually short Si-NBO distance of 1.59 Å. This should contribute to a greater through-bond transfer of unpaired electron spin density from the adjacent Cu^{2+} cation.

The spectra for cuprorivaite also have a small peak centered near to –92 ppm, which required pulse delays of up to 10 s for full relaxation. Under these conditions, its calibrated peak area indicates that it represents about 2% of the total Si in the sample, and could be due to a small amount of a Ca-silicate impurity. The minor cristobalite impurity detected by EPMA and XRD could relax even more slowly and be nearly undetectable by NMR in low concentrations; in contrast, any Cu-rich glass phase that is present (again, suspected at the few % level from EPMA data) could be unobservable in these ^{29}Si NMR experiments because of extreme broadening caused by structural disorder and the accompanying widely varying Cu-Si interactions.

For the main (ca. +720 ppm) peak for the cuprorivaite, the low integrated peak intensity (in the initial spectrum with a 100 μs echo delay) of only about 6 % (Tab. 1) of the expected value cannot be accounted for by incomplete reaction or the presence of impurities, which are estimated from optical microscopy and EPMA imaging to be less than about 5% of the total sample. Experiments with longer pulse delays demonstrate that the main peak is fully relaxed at the 0.1 s pulse delay used; spectra collected with the transmitter frequency centered up to at least 5000 ppm above and below this resonance showed no additional signals. The relatively modest peak width (ca. 7 kHz) did not suggest extreme broadening or signal loss during acquisition.

However, data collected at three different echo delays (1, 2, and 3 MAS rotor periods or 50, 100, and 150 μs) did demonstrate a surprisingly rapid signal decay (Fig. 4). As a first approximation, this decay (measured here as the ratio of the integrated peak area (M) to that expected from the calibration with the diopside standard (M_0)) is expected to be exponential with the echo delay time τ, such that $\ln(M/M_0) \approx -\tau/T_2$. The time constant is the spin-spin relaxation time T_2 (approximated as a constant) and is estimated from the slope to be about 35 μs. When extrapolated back to 0 in the echo delay, the predicted intensity is close to 100% of that expected.

Unlike reduced observable intensities for planchéite, the rapid decay of the signal in cuprorivaite is more likely to be connected to especially fast nuclear spin relaxation, characterized by a short T_2 and probably by a short nuclear spin-lattice relaxation time $T_{1,n}$. In materials with significant contents of paramagnetic centers, relaxation can often be dominated by electron-nuclear interactions, where the *electronic* spin-relaxation time, $T_{1,e}$ plays a key role (Bakhmutov et al. 2009; Grey and Dupré 2004). If $T_{1,e}$ is much shorter than the inverse of the nuclear Larmor frequency ω_L (i.e. the NMR observation frequency for a given nuclide), coupling of the electronic and nuclear spins is inefficient, and relaxation rates are far above minimum values and accompanying peak broadening is not severe. This is often the case for rare earth cations in oxide materials (Grey et al. 1990). $T_{1,e}$ for paramagnetic transition metal cations may be slower, given strong coupling to nuclear spins, faster relaxation, and potentially more severe line broadening. At first glance for the copper silicates studied here, this problem might be expected to be minimized for cuprorivaite, as each Si has only 1 Cu first cation neighbor, in contrast to 3 or 4 for dioptase, shattuckite, and planchéite, thus reducing the total number of interactions between Cu and Si. However, cuprorivaite is distinctive in this group of minerals by

having only isolated CuO_4 groups, instead of continuous chains of edge or corner-shared Cu polyhedra. Interactions among unpaired Cu^{2+} electronic spins are thus likely to be much weaker in cuprorivaite than in the other three minerals. Given that electronic spin-lattice relaxation is likely to be affected or even controlled by these electronic interactions, it is reasonable to hypothesize that the $T_{1,e}$ for cuprorivaite might be relatively slow, promoting more rapid ^{29}Si nuclear spin relaxation and signal loss during acquisition of the NMR signal. Further measurements of T_2, $T_{1,n}$ and $T_{1,e}$ is these types of materials by NMR and EPR methods could prove fruitful for better understanding of such spin dynamics. Details of relaxation rates and mechanisms in paramagnetic systems can also be structurally informative, for example in MnO-containing microporous silica-based materials (Bakhmutov et al. 2009).

Chrysocolla

Chrysocolla is a hydrated, hydroxyl-bearing copper silicate whose formula (neglecting its minor Al content) is often given as approximately $Cu_2H_2Si_2O_5(OH)_4 \cdot xH_2O$ (Hariu et al. 2013). Its weak X-ray diffraction has indicated poor or even non-crystallinity, and thus a poorly defined structure. Much of what we know about this potentially highly variable material thus has come from spectroscopy (e.g. XPS, XAS), including reports on material from the localities of the samples described here (Farges et al. 2007; Frost et al. 2012; Hariu et al. 2013). The goal here is not to resolve all questions about this mineral or "mineraloid", but to test the applicability of paramagnetic ^{29}Si NMR to gain new types of information about its short-range structure, perhaps as a guide to future studies. Our two samples are both from well-studied copper mining centers (Tab. 1) and appear to be mineralogically uniform on microscopic examination, without obvious heterogeneities, color banding, etc.

The ^{29}Si NMR spectra for both samples are nearly identical (Fig. 5), with peak maxima at +380 ppm and linewidths of about 37 kHz (460 ppm); MAS at 20 kHz did not produce significant line narrowing. About 80% of the expected signal is detected. Spectra from both samples also have small, much narrower peaks centered at about –85 ppm with narrow and broader components (line widths about 35 to 80 ppm). These relax more slowly than the main peaks, and are within the range of normal diamagnetic chemical shifts. These may come from small amounts of amorphous silica, probably with minor Cu contents that contribute to widths greater than is typical in the absence of paramagnetic components. The proportions of these impurities are not precisely determined, but peak areas suggest that they comprise less than 10 to 20% of the silica in the samples.

The relatively large paramagnetic shifts for both chrysocolla samples suggest that most of their Si is closely associated with Cu^{2+} cations, with one or more in the first coordination shells. The extreme peak widths are likely the result of disorder as expected in a poorly crystalline material, combined with paramagnetic interactions (^{29}Si peak widths for diamagnetic silicate glasses are typically about 10 to 25 ppm). However, the very similar overall peak positions and shapes for the two samples are unlikely to be the result of a random physical mixture of some type of copper compound (e.g. $Cu(OH)_2$) that is dispersed in amorphous silica or other colloid (Farges et al. 2007), but suggest instead a common stoichiometry and a short- to medium-range structure that is similar in both specimens not only on average but in the overall distribution of Si environments. Such a conclusion has also been reached in experimental studies of synthetic sol-gel products, which although remaining X-ray amorphous, do have reproducible medium-range order (Hariu et al. 2013). Future NMR studies of a wider range of chrysocolla and other "mineraloid" or nano-crystalline silicates is likely to prove interesting.

IMPLICATIONS

New data presented here show that useful ^{29}Si NMR spectra can be observed for several Cu^{2+} silicates, suggesting that there may be a much wider range of applications of this method to a variety of paramagnetic minerals containing cations with unpaired electron spins. Major technical and theoretical challenges remain, however. In some cases, line widths are small enough to be narrowed significantly by magic angle spinning; in others higher resolution spectra will be obtainable with NMR probes with faster spinning rates, which can now reach at least 70 kHz in advanced designs. Rapid spin-lattice relaxation times, which allow for rapid pulsing in the NMR experiment, often allow spectra to be collected with good signal-to-noise ratios even though peaks may be orders of magnitude broader than in diamagnetic minerals. When carefully calibrated with a diamagnetic intensity standard, observed signals may be lower than expected because of very broad peaks and limited excitation bandwidth, or because of rapid signal decay during acquisition in the case of unusually rapid nuclear spin relaxation. Signals can be shifted hundreds to thousands of ppm above or below of the known range for diamagnetic silicates, requiring careful experimental design to even initially determine spectrometer transmitter frequency; temperature variations of 10's of ˚C, induced by air frictional heating during sample spinning, can shift resonances by 100's of ppm. Although as yet we know little about the specific details of the structure that control the large paramagnetic shifts and line widths, these will likely involve the short to medium range relationships between the magnetic cations and Si sites. Potentially important new constraints on bonding, electronic structure, and order/disorder in both pure phases and solid solutions may be obtainable in future studies. Advanced theoretical work, as well as more complex NMR methods that facilitate the accurate detection of very broad NMR

resonances (Pell and Pintacuda 2015), will be especially important in taking full advantage of this newly realized experimental tool.

ACKNOWLEDGEMENTS

This work was supported by the National Science Foundation, EAR-1521055. The author thanks Juan Lezama Pacheco for collecting powder XRD data and Dale Burns for assistance with electron microprobe analyses. We thank two helpful reviewers and the associate editor for useful comments on the manuscript.

REFERENCES

Bakhmutov, V.I., Shpeizer, B.G., Prosvirin, A.V., Dunbar, K.R., and Clearfield, A. (2009) On ^{29}Si NMR relaxation as a structural criterion for studying paramagnetic supermicroporous silica-based materials: Silica-based materials incorporating Mn^{2+} ions into a silica matrix of SiO_2-Al_2O_3-MnO. Solid State Nuclear Magnetic Resonance, 36, 129-136.

Begaudeau, K., Morizet, Y., Florian, P., Paris, M., and Mercier, J.-C. (2012) Solid-state NMR analysis of Fe-bearing minerals: implications and applications for Earth sciences. European Journal of Mineralogy, 24, 535-550.

Bertini, I., Luchinat, C., and Parigi, G. (2002) Magnetic susceptibility in paramagnetic NMR. Progress in Nuclear Magnetic Resonance Spectroscopy, 40, 249-273.

Bloise, A., Abd El Salam, S., De Luca, R., Crisci, G.M., and Miriello, D. (2016) Flux growth and characterization of cuprorivaite: the influence of temperature, flux, and silica source. Applied Physics A, 122, 650-1-8.

Bose, M., Bhattacharya, M., and Ganguli, S. (1979) ^{31}P NMR studies of transferred hyperfine effects in rare-earth orthophosphates. Physical Review B, 19, 72-79.

Bregiroux, D., Audubert, F., Charpentier, T., Sakellariou, D., and Bernache-Assollant, D. (2007) Solid-state synthesis of monazite-type compounds $LnPO_4$ (Ln = La to Gd). Solid State Sciences, 9, 432-439.

Breuer, K.-H., and Eysel, W. (1989) Structural and chemical varieties of dioptase, $Cu_6[Si_6O_{18}].6H_2O$. Zeitschrift für Kristallographie, 187, 15-23.

Carlier, D., Ménétrier, M., Grey, C.P., Delmas, C., and Ceder, G. (2003) Understanding the NMR shift in paramagnetic transition metal oxides using density functional theory. Physical Review, 67, 174103-1-14.

Chakoumakos, B.C., Fernandez-Baca, J.A., and Boatner, L.A. (1993) Refinement of the structures of the layer silicates $MCuSi_4O_{10}$ (M=Ca, Sr, Ba) by Rietveld analysis of neutron powder diffraction data. Journal of Solid State Chemistry, 103, 105-113.

Clément, R.J., Pell, A.J., Middlemiss, D.S., Strobridge, F.C., Miller, J.K., Whittingham, M.S., Emsley, L., Grey, C.P., and Pintacuda, G. (2012) Spin-transfer pathways in paramagnetic lithium transition-metal phosphates from combined broadband isotropic solid-state MAS NMR spectroscopy and DFT calculations. Journal of the American Chemical Society, 134, 17178-17185.

Dogan, F., Vaughey, J.T., Iddir, H., and Key, B. (2016) Direct observation of lattice aluminum environments in Li ion cathodes $LiNi_{1-y-z}Co_yAl_zO_2$ and Al-doped $LiNi_xMn_yCo_zO_2$ via ^{27}Al MAS NMR spectroscopy. ACS Applied Materials and Interfaces, 8, 16708-16717.

Engelhardt, G., and Michel, D. (1987) High-Resolution Solid-State NMR of Silicates and Zeolites. 485 p. Wiley, New York.

Evans, H.T., Jr., and Mrose, M.E. (1977) The crystal chemistry of the hydrous copper silicates, shattuckite and planchéite. American Mineralogist, 62, 491-502.

Farges, F., Benzerara, K., and Brown, G.E., Jr. (2007) Chrysocolla redefined as spertiniite. AIP Conference Proceedings, 882, 223-225.

Frost, R.L., Xi, Y., and Wood, B.J. (2012) Thermogravimetric analysis, PXRD, EDX and XPS study of chrysocolla $(Cu,Al)_2H_2Si_2O_5(OH)_4 \cdot nH_2O$-structural implications. Thermochimica Acta, 545, 157-162.

George, N. C., Pell, A. J., Dantelle, G., Page, K., Llobet, A., Balasubramanian, M., Pintacuda, G., Chmelka, B. F. & Seshadri, R. (2013). Local environments of dilute activator ions in the solid-state lighting phosphor $Y_{3-x}Ce_xAl_5O_{12}$. Chemistry of Materials, 25, 3979-3995.

Grey, C.P., Dobson, C.M., Cheetham, A.K., and Jakeman, R.J.B. (1989) Studies of rare-earth stannates by ^{119}Sn MAS NMR. The use of parmagnetic shift probes in the solid state. Journal of the American Chemical Society, 111, 505-511.

Grey, C.P., and Dupré, N. (2004) NMR studies of cathode materials for lithium-ion rechargeable batteries. Chemical Reviews, 104, 4493-4512.

Grey, C.P., Smith, M.E., Cheetham, A.K., Dobson, R., and Dupree, R. (1990) Y-89 MAS NMR study of rare-earth pyrochlores-paramagnetic shifts in the solid state. Journal of the American Chemical Society, 112, 4670-4680.

Grimmer, A.-R., von Lampe, F., Mägi, M., and Lippmaa, E. (1983) Hochauflösende ^{29}Si-NMR an festen Silicaten; Einfluss von Fe^{2+} in Olivinen. Zeitschrift für Chemie, 23, 343-344.

Hariu, T., Arima, H., and Sugiyama, K. (2013) The structure of hydrated copper-silicate gels, an analogue compound for natural chrysocolla. Journal of Mineralogical and Petrological Sciences, 108, 111-115.

Kim, J., Li, W., Phillips, B.L., and Grey, C.P. (2011) Phosphate adsorption on the iron oxyhydroxides goethite (α-FeOOH), akaganite (β-FeOOH), and lepidocrocite (γ-FeOOH): a ^{31}P NMR study. Energy Environ. Sci., 4, 4298-4305.

Kim, J., Nielsen, U.G., and Grey, C.P. (2008) Local environments and lithium adsorption on the iron oxyhydroxides lepidocrocite (γ-FeOOH) and goethite (α-FeOOH): A ^{2}H and ^{7}Li solid-state MAS NMR study. Journal of the American Chemical Society, 130, 1285-1295.

Law, J.M., Hoch, C., Whangbo, M.-H., and Kremer, R.K. (2010) Description of anhydrous (black) dioptase as a S=1/2 uniform antiferromagnetic chain system. Zeitschrift zur Anorganische und Allgemeine Chemie, 636, 54-61.

Lee, J., Seymour, I.D., Pell, A.J., Dutton, S.E., and Grey, C.P. (2017) A systematic study of ^{25}Mg NMR in paramagnetic transition metal oxides: applications to Mg-ion battery materials. Physical Chemistry Chemical Physics, 19, 613-625.

MacKenzie, K.J.D., and Smith, M.E. (2002) Multinuclear Solid-State NMR of Inorganic Materials. 727 p. Pergamon, New York.

McCarty, R.J., Palke, A.C., Stebbins, J.F., and Hartman, J.S. (2015) Transition metal cation site preferences in forsterite (Mg_2SiO_4) determined from paramagnetically shifted NMR resonances. American Mineralogist, 100, 1265-1276.

McCarty, R.J. and Stebbins, J.F. (2016) Investigating lanthanide dopant distributions in yttrium aluminum garnet (YAG) using solid state paramagnetic NMR. Solid State Nuclear Magnetic Resonance, 79, 11-22.

Michaelis, V.K., Greer, B.J., Aharen, T., Greedan, J.E., and Kroeker, S. (2012) Determining electron spin-transfer mechanisms in paramagnetic Ba_2YMO_6 (M=Mo, Re, Ru) double perovskites by ^{89}Y and ^{137}Ba MAS NMR spectroscopy. J. Phys. Chem. C, 116, 23646-23652.

Middlemiss, D.S., Ilott, A.J., Clément, R.J., Strobridge, F.C., and Grey, C.P. (2013) Density functional theory-based bond pathway decompositions of hyperfine shifts: equipping solid-state NMR to characterize atomic environments in paramagnetic materials. Chemistry of Materials, 25, 1723-1734.

Pabst, A. (1959) Structures of some tetragonal sheet silicates. Acta Crystallographica, 12, 733-739.

Palke, A.C., and Stebbins, J.F. (2011a) Variable temperature ^{27}Al and ^{29}Si NMR studies of synthetic forsterite and Fe-bearing Dora Maira pyrope garnet: temperature dependence and mechanisms of contact-shifted peaks. American Mineralogist, 96, 1090-1099.

Palke, A.C. and Stebbins, J.F. (2011b) Paramagnetic interactions in the ^{31}P NMR spectroscopy of rare earth element orthophosphate ($REPO_4$, monazite/xenotime) solid solutions. American Mineralogist, 96, 1343-1353.

Palke, A.C., Stebbins, J.F., Geiger, C.A., and Tippelt, G. (2015) Cation order-disorder in Fe-bearing pyrope and grossular garnets: An ^{27}Al and ^{29}Si MAS NMR and ^{57}Fe Mössbauer spectroscopy study. American Mineralogist, 100, 536-547.

Pell, A.J., and Pintacuda, G. (2015) Broadband solid-state MAS NMR of paramagnetic systems. Progress in Nuclear Magnetic Resonance, 84-85, 33-72.

Pradell, T., Salvado, N., Hatton, G.D., and Tite, M.S. (2006) Physical processes involved in the production of the ancient pigment, Egyptian blue. Journal of the American Ceramic Society, 89, 1426-1431.

Ribbe, P.H., Gibbs, G.V., and Hamil, M.M. (1977) A refinement of the structure of dioptase, $Cu_6[Si_6O_{18}]\cdot 6H_2O$. American Mineralogist, 62, 807-811.

Saji, H., Yamadaya, T., and Asanuma, M. (1973) Nuclear magnetic resonances of ^{29}Si and long-range superexchange interactions via Co-O-Si-O-Co linkages in Co_2SiO_4. Physics Letters, 45A, 109-110.

Stebbins, J.F., and Kelsey, K.E. (2009) Anomalous resonances in ^{29}Si and ^{27}Al NMR spectra of pyrope ($[Mg,Fe]_3Al_2Si_3O_{12}$) garnets: effects of paramagnetic cations. Physical Chemistry Chemical Physics, 11, 6906-6917.

Stebbins, J.F., McCarty, R.J., and Palke, A.C. (2017) Solid-state NMR and short-range order in crystalline oxides and silicates: a new tool in paramagnetic resonances. Acta Crystallographica C, 73, 128-136.

Stebbins, J.F., and Xue, X. (2014) NMR spectroscopy of inorganic Earth materials. In G.S. Henderson, D. Neuville, and R.T. Downs, Eds. Spectroscopic Methods in Mineralogy and Materials Sciences, 78, p. 605-653. Min. Soc. Am., Chantilly, VA.

Strobridge, F.C., Middlemiss, D.S., Pell, A.J., Leskes, M., Clément, R.J., Pourpoint, F., Lu, Z., Hanna, J.V., Pintacuda, G., Emsley, L., Samosen, A., and Grey, C.P. (2014) Characterizing local environments in high energy density Li-ion battery cathodes: a combined NMR and first principles study of $LiFe_xCo_{1-x}PO_4$. J. Mater. Chem. A, 2, 11948-11957.

Takahashi, T., Kawashima, H., Sugisawa, H., and Baba, T. (1999) ^{207}Pb chemical shift thermometer at high temperature for magic angle spinning experiments. Solid State Nuclear Magnetic Resonance, 15, 119-123.

Tucker, M.C., Doeff, M.M., Richardson, T.J., Finones, R., Reimer, J.A., and Carirns, E.J. (2002) ^{7}Li and ^{31}P magic angle spinning nuclear magnetic resonance of $LiFePO_4$-type materials. Electrochemical and Solid-State Letters, 5, A95-A98.

Yoon, W.S., Iannopollo, S., Grey, C.P., Carlier, D., Gorman, J., Reed, J., and Ceder, G. (2004) Local structure and cation ordering in O3 lithium nickel manganese oxides with stoichiometry $Li[Ni_xMn_{(2-x)/3}Li_{(1-2x)/3}]O_2$. Electrochemical and Solid-State Letters, 7, A167-A171.

Zeng, D., Cabana, J., Bréger, J., Yoon, W.S., and Grey, C.P. (2007) Cation ordering in $Li[Ni_xMn_xCo_{(1-2x)}]O_2$ layered cathode materials: a nuclear magnetic resonance (NMR),

pair distribution function, X-ray absorption, and electrochemical study. Chemistry of Materials, 19, 6277-6289.

Table 1. Samples, ^{29}Si NMR data, and numbers of first neighbor transition metal cations. Site assignments are preliminary estimates. All data are from MAS spectra with 20 kHz spinning speed (≈57 ˚C), 0.1 s pulse delay, and 100 μs echo delay, unless otherwise noted.

sample, locality, formula	peak	site/ phase	no. Cu^{2+}	peak max., ppm	width (FWHM) kHz	relative area[a]
dioptase, SU#1431	A	Si	4	980±20	3.4	0.97±0.05
Altyn Tyube, Kaz.						
$Cu_6(Si_6O_{18})\cdot 6H_2O$						
" 10 kHz spin rate	A	Si	4	1065±20	2.0	
" dehydrated	A	Si	4	895±20	8.6	0.94±0.05
dioptase, SU#7516	A	Si	4	980±20	2.8	0.96±0.05
Guchab, Namibia						
shattuckite, SU#8247	A	Si1?	4	1580±10	9.6	0.46±0.05
Ajo, AZ	B	Si2?	3	–250±10	4.0	0.49±0.05
$Cu_5(SiO_3)_4(OH)_2$						
planchéite, SU#7797	A	Si1+Si4?	4	1200±200	70[b]	A+B+D:
Guchab, Namibia	B	Si2+Si3?	2?	130±20	19[b]	0.74±0.05
$Cu_8(Si_4O_{11})_2(OH)_4\cdot xH_2O$	D	?[d]	?	–120±5	2-4[c]	
cuprorivaite, synthetic	A	Si	1	720±20	7.0	0.06±0.003[f]
$CaCuSi_4O_{10}$						0.24±0.007[f]
	C	?[e]	(0)	–92±5	1.5	0.02±0.01
chrysocolla, SU#8461	A	Si	1-4?	380±20	37[b]	0.7±0.1
Katanga, Zaire	O	a-SiO_2[g]	(0)	–87±5	2-7[c]	≈ 0.03
$\approx Cu_2H_2Si_2O_5(OH)_4\cdot xH_2O$						
chrysocolla, SU#28475	A	Si	2-4?	380±20	37[b]	0.8±0.1
Inspiration mine,	O	a-SiO_2[g]	(0)	–87±5	2.8-7[c]	≈ 0.03
Gila Ct, AZ						
", 4 s pulse delay	A	Si	2-4?	380±20	37[b]	0.8±0.1
	O	a-SiO_2[g]	(0)	–87±5	2.8-7[c]	0.1±0.05

[a] Peak areas include any observed sidebands and are normalized to reported wt% silica, then ratioed to area for Wakefield diopside (SU#31011) standard. Values <1 indicate signal loss.
[b] Spinning speed insufficient for full narrowing.
[c] Composite peak with narrow and broader components.
[d] Possibly an unknown diamagnetic impurity.
[e] Probably Cu-bearing Ca-silicate impurity.
[f] Upper value is for echo delay of 100 μs, lower value is for echo delay of 50 μs.
[g] Probably amorphous silica.

Figure captions

Figure 1. ^{29}Si MAS NMR spectra for copper silicates (Tab. 1). Peaks labeled "A" and "B" are for Si sites in the main phase; "C" may be from a Ca-silicate impurity; "D" may be due to an unknown diamagnetic impurity. "*" marks spinning sidebands. The entire known range of chemical shifts for SiO_4 groups in diamagnetic silicates lies between the two dashed lines. Data shown for cuprorivaite were collected with an echo delay of 50 μs; for others with 100 μs. For planchéite and shattuckite, spectra shown were collected with transmitter frequency centered between two main peaks; for cuprorivaite and dioptase the transmitter frequency was centered on the single main peak.

Figure 2. ^{29}Si NMR spectra for dioptase and dehydrated dioptase, with spinning speeds labeled. The offset of the peak from 20 to 10 kHz (arrow) is caused by a reduction in temperature of about 26 ˚C at the lower spinning speed. The complex MAS peak shapes for the hydrated sample may be due in part to non-uniform temperature in the rotor. Note that the frequency scale is expanded relative to that in Fig. 1.

Figure 3. Local structures around the Si sites in representative copper silicates. In shattuckite ($Cu_5(SiO_3)_4(OH)_2$), Si1 (a) and Si2 sites (b) are linked to form corner-shared chains; nearly planar CuO_4 groups are edge and corner shared, also to form chains. Si1 has four close Cu neighbors; Si2 has three. H positions are not shown. In cuprorivaite ($CaCuSi_4O_{10}$) (c), each Si has three Si and only one CuO_4 neighbor, which is isolated from other Cu. Ca site is not shown. (Color online.)

Figure 4. Natural logarithm of the observed, integrated ^{29}Si NMR signal intensity (M) for cuprorivaite and planchéite, normalized to that expected from the pure diopside standard (M_0), vs. the echo delay time in μs. For cuprorivaite, extrapolation back to zero delay gives a ratio close to 1 (i.e. $\ln(M/M_0) = 0$), i.e. the full expected intensity. For planchéite, signal loss is less severe but is not a strong function of delay time and does not extrapolate to the full expected value.

Figure 5. ^{29}Si MAS NMR spectra for two chrysocolla samples (Tab. 1), with the same ppm scale as Fig. 1. Peaks marked "O" are probably due to amorphous "opaline" silica. Pulse delays are noted. The entire known range of chemical shifts for SiO_4 groups in diamagnetic silicates lies between the two dashed lines.

FIGURE 1

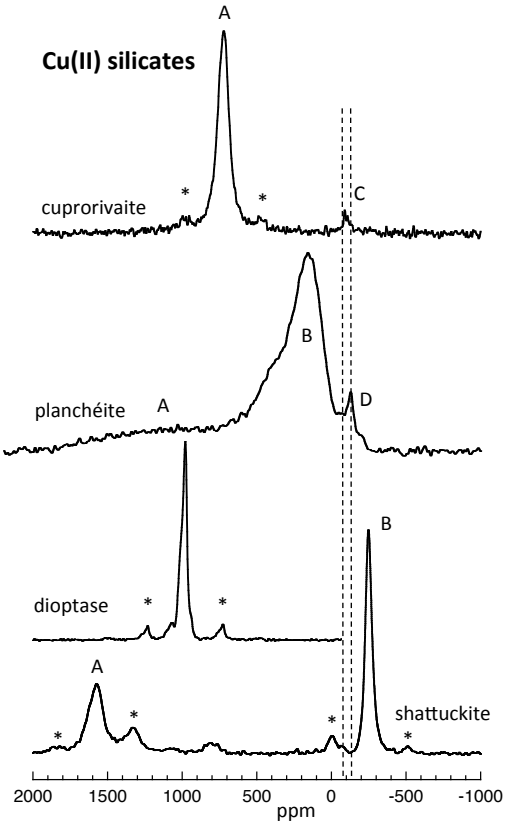

FIGURE 2

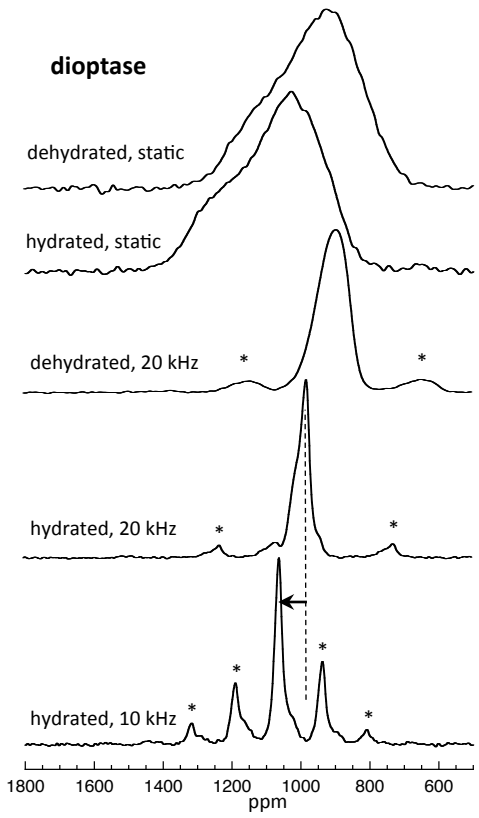

FIGURE 3

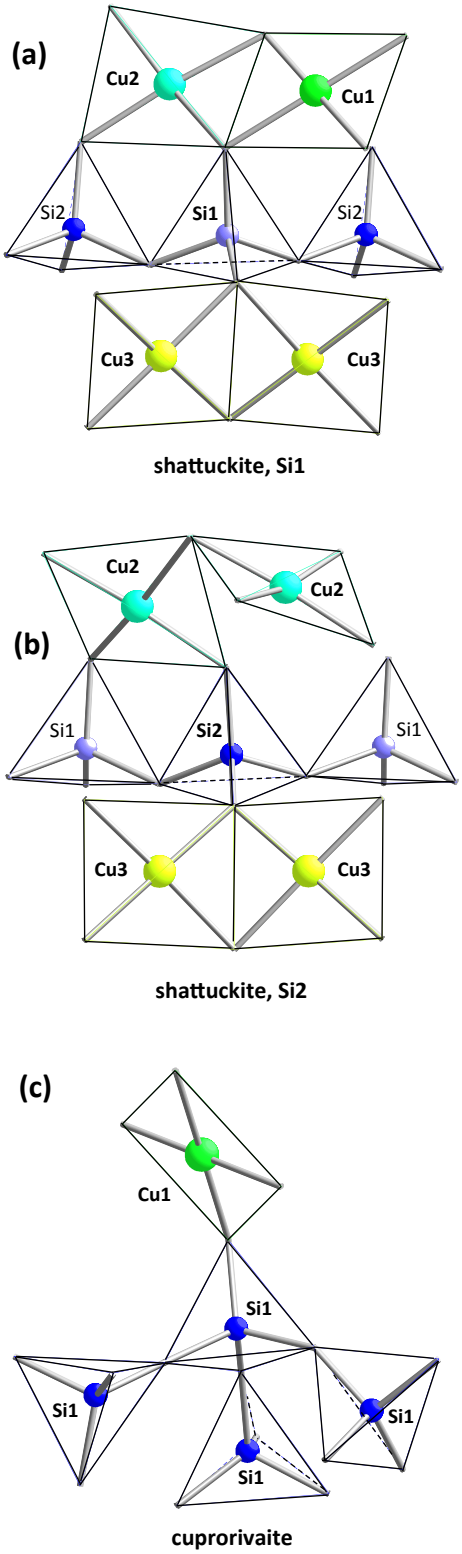
(a)
Cu2
Cu1
Si2
Si1
Si2
Cu3
Cu3
shattuckite, Si1
(b)
Cu2
Cu2
Si1
Si2
Si1
Cu3
Cu3
shattuckite, Si2
(c)
Cu1
Si1
Si1
Si1
Si1
cuprorivaite

FIGURE 4

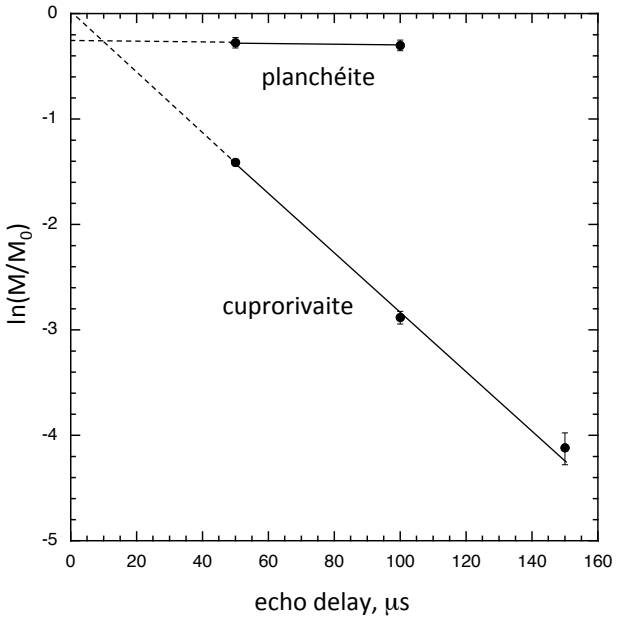
0
-1
-2
-3
-4
-5
ln(M/M0)
planchéite
cuprorivaite
0
20
40
60
80
100
120
140
160
echo delay, μs

FIGURE 5